Centrifuge modelling of the effects of soil liquefiability on seismic response of low-rise structures

Qi, Shengwenjun; Knappett, Jonathan

Published in:
Physical Modelling in Geotechnics

DOI:
10.1201/9780429438646

Publication date:
2018

Document Version
Peer reviewed version

Author Accepted Manuscript version of Qi, S & Knappett, J 2018, Centrifuge modelling of the effects of soil liquefiability on seismic response of low-rise structures. in A McNamara, S Divall, R Goodey, N Taylor, S Stallebrass & J Panchal (eds), Physical Modelling in Geotechnics : Proceedings of the 9th International Conference on Physical Modelling in Geotechnics (ICPMG 2018), July 17-20, 2018, London, United Kingdom. 1 edn, vol. 2, CRC Press, London, pp. 1011-1016, 9th International Conference on Physical Modelling in Geoetchnics, London, United Kingdom, 17/07/18. Final version available https://doi.org/10.1201/9780429438646

Centrifuge modelling of the effects of soil liquefiability on the seismic response of low-rise structures

S. Qi, & J.A. Knappett
School of Science and Engineering, University of Dundee, UK

ABSTRACT: Earthquake-induced soil liquefaction can generate significant damage to low-rise structures, as evidenced in the 2010-2011 Canterbury Earthquake Sequence in New Zealand. In this paper, the structural response of low-rise structures on medium dense granular soils of different permeability (but both nominally liquefiable) was investigated using dynamic centrifuge modelling. In the tests, a series of consecutive motions from the 2010-2011Canterbury Earthquake Sequence was considered, followed by a long duration 'double-pulse' motion from the 2011 Tohoku Earthquake which can potentially apply large inertial loads after liquefaction has been triggered. It was observed that the lower permeability test reached full liquefaction at shallow depth during shaking, while soil of higher permeability was only comparable in response in the first earthquake; in subsequent strong aftershocks excess pore water pressures were substantially reduced. The structural response of higher permeability soil was 10-45% larger due to the increased motion transmission ability of the soil after the initial earthquake. The structure on the higher permeability soil did, however, show reduced post-earthquake tilt in all motions tested. These results suggest that popular liquefaction triggering analyses may be limited in their ability to properly estimate the hazard posed to structures on nominally liquefiable soil when estimating resistance to subsequent motions (aftershocks).

1 INTRODUCTION

During earthquakes, the effect of soil liquefaction can cause very damaging effects in low-rise structures. An increase in excess pore water pressure (EPWP) can occur across a range of particle size distributions and relative densities in granular soils, which can result in different amounts of liquefaction in soils which are all nominally liquefiable. Earthquake induced liquefaction generally damages structures as a result of a loss of effective overburden stress within soil with EPWP generation, resulting in excessive settlement and tilting of structures with shallow foundations, as evidenced in 2010-2011 Canterbury Earthquake sequences (e.g. Cubrinovski et al. 2012).

The consequence of liquefaction induced damage on foundation can depend on a series of uncertainties (e.g. earthquake loading, site condition and the superstructure). There is lack of analytical methods cooperating effects of deviatoric and volumetric settlements together to evaluate foundation settlements when soil softens (Dashti et al. 2010). Physical modelling using centrifuge is a way of studying effects of liquefaction on building performance. Previous studies have generally considered settlement of shallow foundations alone or as a rigid structure with a centred mass representing the structure on liquefiable soil (Liu & Dobry, 1997, Dashti et al. 2010, Bertalot & Brennan, 2015) or as a more representative flexible structure with stiffness and mass but on non-liquefiable sand (e.g. Knappett et al. 2015). This paper aims to bring these two effects together, considering a wider structural response (co-seismic structural acceleration, inter-storey sway and drift, within a multi-degree of freedom structural system), alongside the foundation response in terms of post-earthquake settlement and tilt of a two-storey structure with strip foundations on soils of different permeability but similar pre-earthquake stiffness and strength. Through the comparison of high and low permeability subsoil, and the application of multiple earthquakes of different acceleration magnitudes it will be possible to examine: (i) the effect of the degree of liquefaction occurring; and (ii) the influence of pre-shaking and

aftershocks on the linked structural and geotechnical performance of the structure in liquefiable soil.

Two dynamic centrifuge tests are presented here, consisting of the same single two-storey structure with separated strip foundations on two different permeability sands of similar relative density (i.e. so the foundations in each case have the same static factor of safety). The input ground motions considered in the two tests are a re-ordered sequence of motions from the Canterbury Earthquake Series of 2010-2011 followed by a long duration 'double-pulse' record from the 2011 Tohoku Earthquake.

2 CENTRIFUGE MODELLING

The two centrifuge tests were conducted using a model scale of 1:40 and tested at 40-g using the 3.5m radius geotechnical centrifuge at the University of Dundee. A full description of centrifuge scaling can be found in Muir wood (2004).

2.1 *Model structure*

The structural model was designed to represent a two-storey, single bay, steel moment resisting frame with concrete slabs sitting on separated concrete strip foundations which is a typical damaging building type in Christchurch residential area (Cubrinovski et al. 2012). Square aluminium alloy rods were used to form individual model columns, while aluminium alloy plates were used to create the floor slabs, with additional steel plates bolted to these to allow the floor mass to be varied in later adjacent structure tests (though this feature is not used within the tests described herein). The strip foundations were also made of aluminium plates due to the close similarity in unit weight between this material and reinforced concrete. The foundation width used provides a static factor of safety of 3 against bearing failure, accounting for the total self-weight and a 3.5 kPa extra loading on each storey (applying a bearing pressure of 50 kPa on each footing). The model structure is shown in Figure 1.

The fundamental natural period of the steel frame at prototype scale was targeted using Equation 1:

$$T_n = 0.1N \quad (1)$$

where N is the number of stories of the structure (N = 2 and $T_n \approx 0.2$ s here).

The mass of each floor (all in prototype) was determined based on a 3.6 m × 3.6 m × 0.5 m concrete slab (where the masses of each floor are the same, i.e. $M_1 = M_2$). The equivalent stiffness of the structure in the fundamental mode was then determined by combining Equation 1 and Equation 2, setting the columns of each storey to have the same to have the same stiffness, i.e. $K_1 = K_2$), and selecting the closest available steel Universal Column size to provide an appropriate amount of bending stiffness EI:

$$T_n = 2\pi\sqrt{\frac{M_{eq}}{K_{eq}}} \quad (2)$$

where:

$$M_{eq} = M_1\,\overline{y_1}^2 + M_2\,\overline{y_2}^2 \quad (3)$$

$$K_{eq} = K_1(\overline{y_1})^2 + K_2(\overline{y_2} - \overline{y_1})^2 \quad (4)$$

The normalized modal coordinates associated with the fundamental mode were $\overline{y_1}$ = 0.45 and $\overline{y_2}$ = 0.89, based on an eigenvalue analysis for the two-storey structure with equal stiffness and mass at each storey. The final natural period of the two-storey building was 0.21s. A summary of properties at prototype is shown in Table 1.

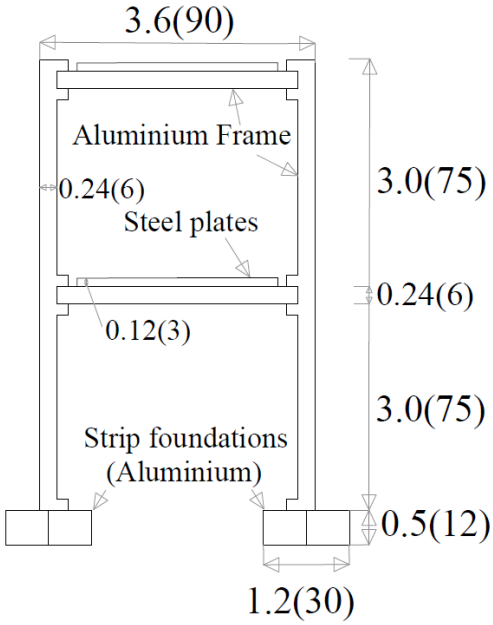

Figure 1 Model structure: dimensions at prototype scale are shown in m; dimensions at model scale are given in mm in brackets ().

Table 1.Section properties (prototype scale)

Element	Description	Property
Concrete slab	3.6m×3.6m×0.5m (C25 concrete)	M_1=M_2=16.5×10^3 kg
Steel column	203×203×86 UC (3m storey height)	EI=20.9×10^6 Nm^2 K_1=K_2=37.1×10^6N/m
Concrete strip foundations	1.2m×4.8m×0.5m (C25)	M_f=7.3×10^3 kg/strip

2.2 *Model preparation and soil properties*

8 m deep deposits of dry HST95 Congleton silica sand layer (D_r=55%-60%) were initially air-pluviated into an equivalent shear beam (ESB) container in

each test and saturated using water or hydroxyl-propyl methyl-cellulose (HPMC) pore fluid (providing a factor of 40 difference in permeability). The soil with HPMC provides a soil of comparatively lower permeability, while the water saturated soil represents a soil of comparatively higher permeability. Further information regarding the ESB container can be found in Bertalot, (2013). The container was designed for normal use at 50-g in the centrifuge, so does not represent a perfect boundary for the 40-g tests considered here. However, any unwanted boundary effects were minimised by placing the structure close to the centre of the container and far from the end walls (see Coelho et al. 2003). Physical properties of the HST95 sand are listed in after (Lauder, 2010).

The soil model was instrumented during pluviation with accelerometers and pore pressure transducers in five layers as shown in Figure 2 to measure the EPWP generation and accelerations in the free-field (full-depth, points A-E) and beneath the structures (at the same depth as free-field instrumentation, i.e. point F). Saturation using vacuum technique to reduce air bubbles in the soil in this specific case is not possible due to the presence of weakly glued latex membrane placed on the internal walls of the model container. This was instead achieved by allowing de-aired fluid to enter the model under a constant gravitational head through the bottom of the ESB container at a relatively low flow rate until it reached 2 mm above the model surface. Based on the slow speed of saturation (Bertalot, 2013) and the volume of fluid entering the model it was possible to achieve conditions close to full saturation.

After loading the ESB container with saturated soil onto the centrifuge, the instrumented structure was placed carefully on the surface of the soil to be as level as possible; any initial tilt was measured using a clinometer to provide a baseline for subsequent measurements of structural rotation. MEMS Accelerometers were attached to the structures on each floor and at the foundations to measure the vertical and horizontal accelerations on each foundation and each storey (see Figure 2 for positions). Dynamic inter-storey sway and drift data were determined through careful filtering and integration of the accelerometer data. Two linear variable differential transformers (LVDTs) fixed on an overhead gantry were placed on top of model structure to measure average settlement and global rotation (tilt).

Table 2 Physical properties of HST95 Congleton sand (Lauder, 2010)

Property	Value
Specific gravity, G_s	2.63
D_{10}: mm	0.09
C_u (uniformity) and C_z (curvature)	1.9 and 1.06
Maximum void ratio, e_{max}	0.769
Maximum void ratio, e_{min}	0.467

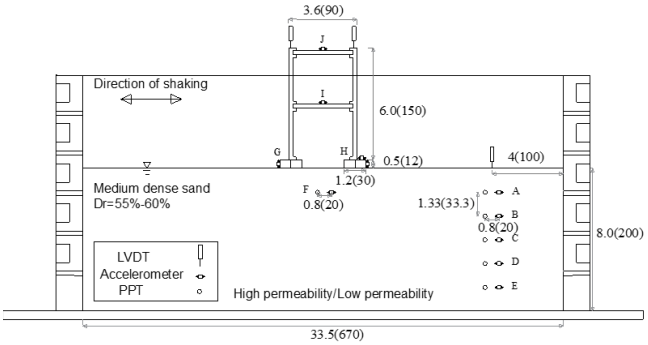

Figure 2 Layout of centrifuge test: dimensions in prototype are shown in m; dimensions in model scale are shown in mm in brackets ().

2.3 *Dynamic Excitation*

Following spin-up, a re-ordered sequence of motions from the Canterbury Earthquake Sequence 2010-2011 (motions recorded at the Christchurch Botanical Gardens Station from Pacific Earthquake Engineering Research database) followed by a long duration 'double-pulse' motion rom the 2011 Tohoku Earthquake (recorded at Ishinomaki Station from National Research Institute for Earth Science and Disaster Resilience). These were applied in sequence using the Actidyn QS67-2 servo-hydraulic earthquake simulator (EQS) at the University of Dundee. The motions were filtered using an eighth order Butterworth filter with a band pass between 2.3-7.5Hz (at prototype scale). The filtered time histories of input acceleration and peak ground acceleration (PGA) values are shown in Figure 3.

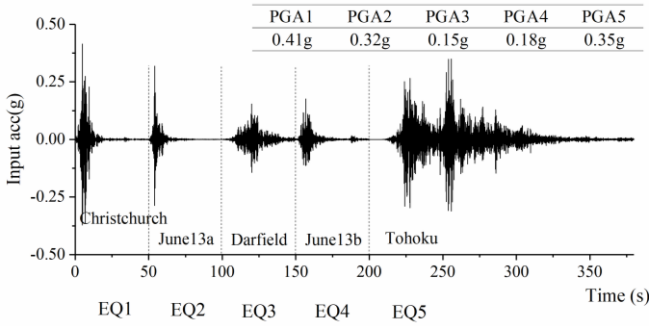

Figure 3 Input acceleration time history and peak ground acceleration (PGA)

It was decided to apply the Christchurch Earthquake (February 2011) first as this was observed to have induced the most severe liquefaction-induced damage in the Canterbury Earthquake Sequence, and by occurring first, the initial state of the soil is fully known in the tests. Three subsequent motions from the same station ('June13a' from 2011, Darfield from 2010 and 'June13b', also from 2011) were then applied in order of expected lower EPWP generation, providing strong aftershocks generating different amounts of liquefaction. The last applied Tohoku mo-

tion was intended to be strong enough and with sufficient duration to fully re-liquefy the soil, even if the previous motions caused significant densification of the soil and reduction in liquefaction potential. This motion is also of particular interest as there are two distinct pulses of high PGA. Therefore, while in the initial Christchurch motion the early strong shaking will generate liquefaction, but thereafter apply smaller inertial demands on the structure, the final Tohoku motion can liquefy the soil and then apply a strong pulse in the liquefied state, which may be a more detrimental extreme loading case for the structure.

3 RESULTS

Results for EPWP generation and accelerations in the free-field and beneath the structure, structural response and foundation deformation will be discussed in this section. Some key performance indicators are summarized as follows: (1) excess pore pressure ratio r_u in the free-field and beneath the structure; (2) peak storey acceleration at storey 1 (point I); (3) peak cyclic sway at storey 1; (4) peak cyclic inter-storey drift (i.e. where dynamic rocking induced displacements have been subtracted from sway data) across storey 1; (5) post-earthquake settlement and (6) structural tilt. Structural response quantities focus on storey 1 as a two-storey structure with uniform mass and stiffness distribution with height will see the largest structural deformation (inter-storey drift) within the first storey. This point is also close to the centre of mass of the structure. All data presented in this section are at prototype scale, unless otherwise stated.

3.1 *Excess pore water pressure generation*

Pore pressure transducers were located in the free-field and beneath the structure (Figure 2). All EPWP readings were continuously recorded from before the start of earthquake shaking until the EPWP had fully dissipated. For the lower permeability test this required a relatively long recording time (4 minutes at model scale) compared to the higher permeability test. The readings have been corrected according to the placed initial position and instrument displacement during saturation (inferred from the static pore water pressures observed during spin-up) and between earthquake motions (based on any final static offset in the EPWP measurement after the EPWP had fully dissipated, i.e. $dr_u/dt = 0$).

Excess pore pressure ratio r_u is the maximum increase in EPWP divided by the in-situ effective vertical stress at the same depth. Figure 4 shows a comparison of free-field r_u with depth (round markers with black or grey line connected) and r_u beneath the structure (square markers without line connected) in the two tests. A reduction in r_u with depth can be generally observed in all EQs in the high permeability test (grey line) and in the aftershock motions EQ2-4 in the low permeability test (black line).

In the first earthquake, both soils show similar values of r_u down to 5 m depth. However, in all subsequent aftershocks, the higher permeability soil generally experienced much lower generation of EPWP due to the increased ability of the soil to rapidly dissipate EPWP as it is generated in a soil that is continually densifying during post-earthquake reconsolidation. This case only reaches full liquefaction near the surface in EQ1, and partial EPWP generation afterwards; however, the lower permeability soil reaches full liquefaction at essentially all depths in EQ1, and is fully re-liquefied at all depths in EQ5. The difference in EPWP resulted in greater soil softening in the lower permeability soil, which could be seen in the accelerations transmitted to the ground surface and on to the structure (Figure 5).

By comparing square markers to free-field values in Figure 4, the EPWP generation beneath the foundation is generally smaller (or equal in stronger earthquakes) than the free-field value, which has previously been observed by Bertalot & Brennan (2015) for foundation-only models and attributed to the foundation bearing pressure increasing the confining effective stresses and inhibiting liquefaction.

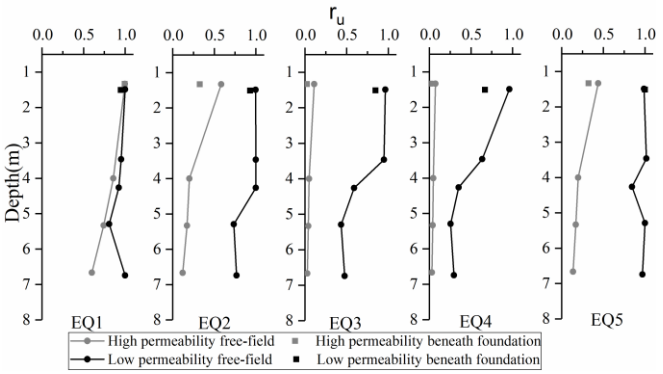

Figure 4 Excess pore pressure ratio (r_u) along depth

3.2 *Structural response*

All accelerations were filtered through a high pass zero phase-shift filter. Examples of acceleration time history are shown in Figure 5. The acceleration transmitted to the top free-field accelerometer is shown in Figure 5(a). By comparing the black and grey overlap, it can be observed that less acceleration was transmitted to the top in the low permeability soil due to the much higher EPWP. Storey1 acceleration in Figure 5(b) also lower in the low permeability case due to soil softening caused by liquefaction.

Inter-storey sway across the first storey ('sway01') is the horizontal displacement of storey 1 relative to that of the foundations during shaking. The displacement was derived by high pass filtering and double integration of the accelerometer data at point G, H and I in Figure 2. The relative sway between storey 1 and

the foundations was then derived by subtracting the average displacement of point H and I from point G.

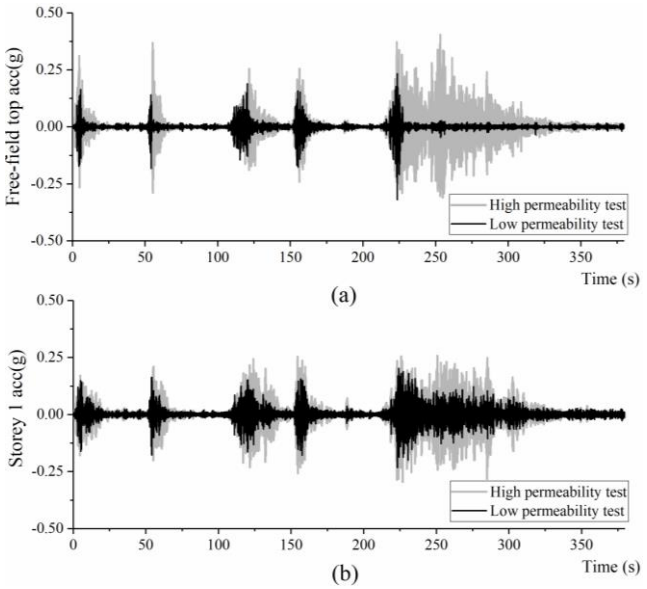

Figure 5 (a) Free-field top acceleration time history; (b) Storey 1 acceleration time history

The sway data is a combination of pure horizontal structural deformation (inter-storey drift, i.e. relative lateral movement between the two ends of the columns due to bending) and dynamic rocking induced displacement. Inter-storey drift (here 'Drift01') is a better indicator of the likelihood of structural damage to the building frame or any infill/curtain walling systems, as it is a direct measure of structural distortion. Dynamic rocking was derived through a high pass filtering of the rotation data (described in section 3.3) to obtain only the dynamic shaking component, excluding the permanent rotation caused by bending deformation.

Figure 6 shows the peak sway, inter-storey drift and storey acceleration during each earthquake at or across storey 1. A general reduced structural dynamic response (by 10%-45%) is observed in the lower permeability case. This is consistent with the more extensive soil softening caused by greater EPWP generation in the lower permeability test. The weaker soil can transmit less acceleration so less inertial force was transferred to the structure resulting in this reduced response. It can also be seen that this reduction is much larger for sway (which includes the peak dynamic rotation) compared to inter-storey drift (which does not). This suggests, counter-intuitively, that there is greater rocking/dynamic rotation in the soil with lower EPWP, which dissipates more of the input energy to the structure, resulting in lower drift. This may be because the increased inertial actions in the structure out-weigh the potential for increased cyclic foundation vertical movement in soil with higher EPWP. The peak vertical acceleration of the foundations and the induced vertical displacement here are shown in Figure 7, indicating the dynamic rocking of the foundations during shaking in each case which support this conclusion.

It is also noticeable that similar dynamic response occurs in both soils in EQ1 for all structural measures, and the differences between responses become apparent in the subsequent earthquakes (aftershocks). This is consistent with both models exhibiting similar EPWP distribution in EQ1 (Figure 4) and illustrates that differences in soil liquefiability may mainly complicate understanding of the response in aftershocks, i.e. in post-earthquake assessment of the resilience of an affected structure to future events.

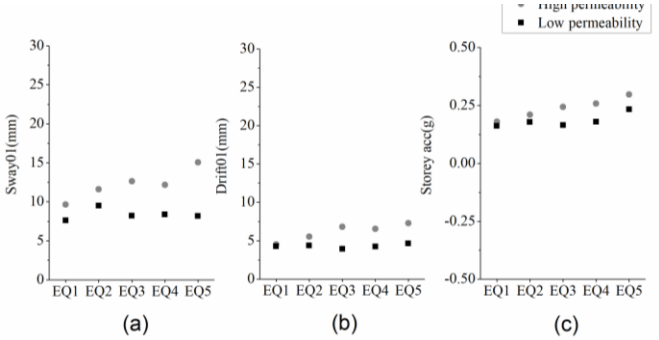

Figure 6 (a) Inter-storey sway01; (b) inter-storey drift01; (c) Storey acceleration

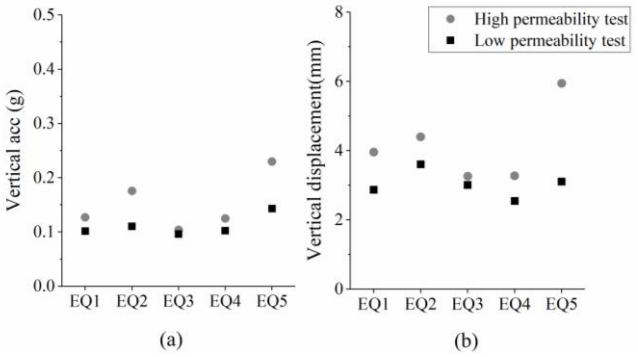

Figure 7 (a) Peak vertical acceleration on the foundation; (b) Peak vertical displacement on the foundation

3.3 *Earthquake induced Settlement and tilt*

Settlement and tilt of a structure are measurements of the foundation performance during earthquakes. Large values would potentially influence the post-earthquake serviceability of a structure, even if the superstructure is largely undamaged. Both of these pieces of data were derived from synthetic LVDT data, because the LVDT alone cannot represent the shaking induced vertical displacement accurately. Figure 8 is an example of synthetic LVDT data showing part of the time history in the final Tohoku motion (EQ5). The LVDT data was first low-pass filtered so that only the monotonic component was left in the data (Figure 8(a)); then the double integrated vertical accelerometer data for the instruments mounted on the foundations, representing the vertical dynamic component (Figure 8(b)) are added. The final synthetic LVDT data was used in interpreting settlement, (through averaging to values of the two foundations)

and rotation (from the difference in measurements across the foundation).

Figure 9(a) shows greater post-earthquake relative settlement in the high permeability case (except for the last EQ), possibly caused by the greater acceleration transfer induced dynamic rocking and inertial force due to the lower EPWP generation at depth discussed in 3.1 and 3.2. This greater stamping effect in the higher permeability test appears to result in larger settlements than the sinking caused by high EPWP in the low permeability case, which is a surprising observation.

The higher permeability case in Figure 9(b) does, however, rotate relatively less compared to the low permeability case, and rotation is perhaps more critical to post-earthquake serviceability than gross settlement. This suggests that structural performance in liquefiable soil is a trade-off between larger structural demand but better foundation performance, or vice-versa, particularly in strong aftershocks.

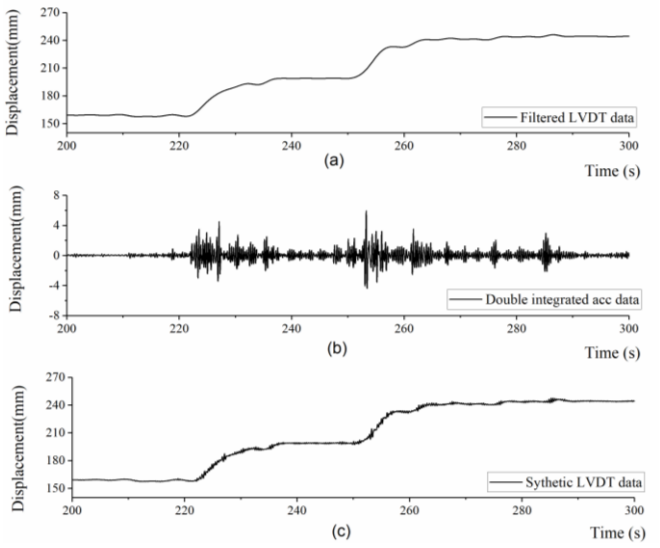

Figure 8 (a) Low-pass filtered LVDT data; (b) Double integrated acceleration data; (c) Synthetic (combined) LVDT data

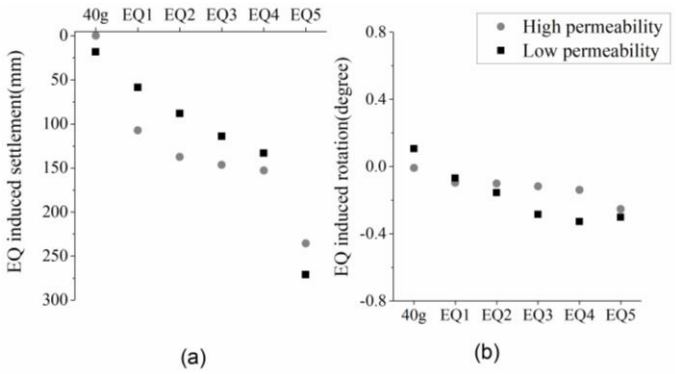

Figure 9 (a) Cumulative earthquake-induced settlement; (b) Cumulative earthquake-induced rotation

4 CONCLUSIONS

This paper has investigated how soil permeability may influence the seismic response of low-rise structures for soils which are nominally liquefiable. A two-storey true multi-degree of freedom model was used in centrifuge tests so that both structural demand and foundation performance could be evaluated and compared, during a sequence of strong motions.

It was shown that in the first/initial earthquakes that both soils showed similar EPWP generation and structural demand. However, in subsequent strong aftershocks, soils of higher permeability exhibited much lower EPWP generation at depth, resulting in increased structural demand (by 10-45%, depending on the motion) and increased settlement due to greater foundation 'stamping'; however, post-earthquake rotation was reduced significantly.

These results indicate that even if the potential for liquefaction can be established through a liquefaction triggering analysis, it may remain difficult to estimate the consequences of an earthquake (particularly an aftershock) and therefore estimate damage potential, as the structural and foundation response depends on the EPWP that is developed.

5 REFERENCES

Bertalot, D. 2013. Foundations on layered liquefiable soils. PhD thesis, University of Dundee, Dundee, UK.

Bertalot, D. and Brennan, a. J. 2015. foundations Influence of initial stress distribution on liquefaction-induced settlement of shallow foundations. Géotechnique, 65(5), 418-428. doi: 10.1680/geot.SIP.15.P.002.

Coelho P, Haigh SK and Madabhushi SG. Boundary effects in dynamic centrifuge modelling of liquefaction in sand deposits. Proceedings of the 16th ASCE engineering mechanics conference, University of Washington, Seattle, USA, 2003: 1-12.

Cubrinovski, M., Henderson, D., & Bradley, B. 2012. Liquefaction impacts in residential areas in the 2010–2011 Christchurch earthquakes. Proceedings of International Symposium on Engineering Lessons Learned from the 2011 Great East Japan Earthquake, 811-824.

Dashti, S., Bray, J.D., Pestana, J.M., Riemer, M.R. and Wilson, D. 2010. Centrifuge Testing to Evaluate and Mitigate Liquefaction-Induced Building Settlement Mechanisms. Journal of Geotechnical and Geoenvironmental Engineering 136(7): 918-929.

Dashti, S., Bray, J.D., Pestana, J.M., Riemer, M.R. and Wilson, D. 2010. Mechanisms of seismically-induced settlement of buildings with shallow foundations on liquefiable soil. J. Geotech. Geoenviron. Engng., ASCE, 136 (1):151-164

Knappett, J. A., Madden, P. and Caucis, K. 2015. Seismic structure–soil–structure interaction between pairs of adjacent building structures, Géotechnique, 65(5), pp. 429–441. doi: 10.1680/geot.SIP.14.P.059.

Lauder, K. 2010. The performance of pipeline ploughs The performance of pipeline ploughs. PhD thesis, University of Dundee, Dundee, UK

Liu, L. and Dobry, R., 1997. Seismic response of shallow foundation on liquefiable sand. Journal of Geotechnical and Geoenvironmental Engineering, ASCE, 123(6), 557-567.

Muir Wood, D. 2004. Geotechnical modelling. London, UK: Spon Press, Taylor and Francis.